JPE 17-4-15

https://doi.org/10.6113/JPE.2017.17.4.991
ISSN(Print): 1598-2092 / ISSN(Online): 2093-4718

Global Sliding Mode Control based on a Hyperbolic Tangent Function for Matrix Rectifier

Zhanhu Hu[*,**], Wang Hu[*], Zhiping Wang[†], Yunshou Mao[*], and Chenyang Hei[***]

[*]School of Automation, Guangdong University of Technology, Guangzhou, China
[†,**]Guangdong Institute of Intelligent Manufacturing, Guangzhou, China
[***]School of Electric Power, South China University of Technology, Guangzhou, China

Abstract

The conventional sliding mode control (CSMC) has a number of problems. It may cause dc output voltage ripple and it cannot guarantee the robustness of the whole system for a matrix rectifier (MR). Furthermore, the existence of a filter can decrease the input power factor (IPF). Therefore, a novel global sliding mode control (GSMC) based on a hyperbolic tangent function with IPF compensation for MRs is proposed in this paper. Firstly, due to the reachability and existence of the sliding mode, the condition of the matrix rectifier's robustness and chattering elimination is derived. Secondly, a global switching function is designed and the determination of the transient operation status is given. Then a SMC compensation strategy based on a DQ transformation model is applied to compensate the decreasing IPF. Finally, simulations and experiments are carried out to verify the correctness and effectiveness of the control algorithm. The obtained results show that compared with CSMC, applying the proposed GSMC based on a hyperbolic tangent function for matrix rectifiers can achieve a ripple-free output voltage with a unity IPF. In addition, the rectifier has an excellent robust performance at all times.

Key words: DC output voltage, Global sliding mode control, Hyperbolic tangent function, Input power factor, Matrix rectifier

I. INTRODUCTION

The matrix rectifier, which is deduced from a three-phase AC/AC matrix converter (MC), is a general three-phase AC/DC buck power converter [1]. The advantages of this converter are its sinusoidal input current waveform, controllable input power factor, bidirectional energy flow, operation in all four quadrants, no large energy storage elements, etc [2]. Because of the above features, the MR has become a hot spot in the field of power electronics, and has been widely studies by a lot of experts and scholars [3]-[5].

However, space vector modulation (SVM) algorithms which are commonly used for the MR is an open-loop control [6]. The dc output voltage of the rectifier is sensitive to external disturbances and parameter variations, which seriously affect the industrial applications of the MR.

Manuscript received Oct. 22, 2016; accepted Apr. 3, 2017
Recommended for publication by Associate Editor Sangshin Kwak.
[†]Corresponding Author: 326863210@qq.com
Tel: +82-20-87682474,Guangdong Inst. of Intelligent Manufacturing
[*]School of Automation, Guangdong University of Technology, China
[**]Guangdong Institute of Intelligent Manufacturing, China
[***]School of Electric Power, South China Univ. of Technology, China

Meanwhile, in order to suppress high-order harmonics and to improve the quality of the waveforms, an input filter is an essential part of a MR system. Due to the input filter's characteristic, the IPF can be obtained near unity only in the case of high output loads, and the IPF is significantly decreased under low output load conditions. As a result, the fixed compensation method is not accurate enough and is not suitable for the rectifier [7].

To mitigate the influence of the above problems, the authors of [8]-[11] proposed several control strategies to achieve a tight dc output voltage with a high IPF under normal and non-normal conditions. However, traditional control strategies, such as input feedforward and output feedback, make it difficult to eliminate low frequency fluctuations of the output voltage, and their dynamic compensation performance is poor. For the sake of obtaining a quick response and robustness, a SMC strategy was applied in [12]-[14]. Although the dynamic response time is better than that with PI control, the chattering in the sliding mode is larger, the output waveform is distorted, and redesigning the switching table makes the calculation more complex. To further eliminate the chattering and simplify the calculation, SMC methods based on the reaching law and

uncertain parameters were introduced in [15], [16], respectively. In order to obtain an optimal control function, an accurate detection for the internal parameters is needed in the reaching law, which increases the difficulty of the implementation. Moreover, these SMCs are established with discontinuous functions, which cannot be fundamental to suppress the sliding mode chattering.

In addition, due to the CSMC system including reaching phase and sliding phase, the MR does not have robustness in the reaching phase. As a result, it cannot guarantee robustness in the whole system. A SMC based on the exponential reaching law was used in [15] and [17], which could shorten the time of the reaching phase. However, the reaching phase still existed. Therefore, [18] and [19] proposed a dynamic nonlinear sliding surface to remove the reaching phase. They also presented a design method for the global switching function. Moreover, in [20] and [21], the GSMC was used in a Buck converter and a single-phase photovoltaic grid-connected inverter, and promoted the development and application of the global sliding mode in the converter control field. However, the global sliding mode applied in a matrix rectifier has not been reported in the literature.

In accordance with the continuous and smooth characteristics of the hyperbolic tangent function and the global robustness in the global sliding mode, on the basis of the SVM and its static analysis in the DQ model for a MR, this paper presents a novel strategy by applying GSMC and SMC based on a hyperbolic tangent function to regulate the tight dc output voltage and to compensate the IPF, respectively. The proposed approach can ensure that the rectifier has global robustness with a unity IPF, and that the dc output voltage chattering can be suppressed well, which improves the waveform quality of the output voltage effectively. In addition, ripple-free output voltage can be obtained with a unity IPF even if the input voltage is distorted.

The paper is organized as follows. Section II introduces the topology and SVM strategy of a MR in detail. A GSMC model for the dc output voltage is analyzed and designed in Section III. The IPF is compensated by a SMC strategy in section IV. In section V, simulations and experimental results are presented, and a summary is presented in Section VI.

II. Matrix Rectifier and its Modulation Strategy

The topological construction of a MR is shown in Fig. 1. It consists of a three phase power supply, an input filter, a switch array with six bi-directional switches, an output filter and a load.

When using SVM for a MR, the six bi-directional switches should be feasible so that each output phase has one and only one ON-state switch at any time instance. Thus, it is divided into six non-zero vectors ($I_1 \sim I_6$) and three zero vectors ($I_7 \sim I_9$). The space vector hexagon is separated into

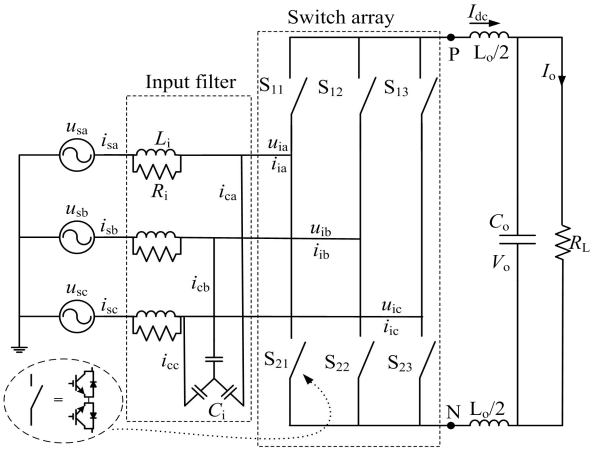

Fig.1. Topology of the MR.

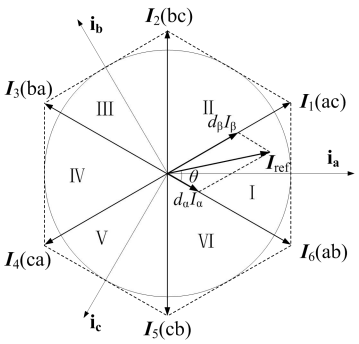

Fig.2. Space vector diagram of the input current.

six sectors by the non-zero vectors, and the dc output voltage is synthesized from two adjacent vectors and a zero vector. The synthesis principle is shown in Fig. 2 and can be calculated as:

$$I_{\text{ref}} = \frac{T_\alpha(\theta)}{T_s} I_\alpha + \frac{T_\beta(\theta)}{T_s} I_\beta + \frac{T_0(\theta)}{T_s} I_0 \tag{1}$$

where I_{ref} is the reference current vector, and I_α and I_β are two adjacent vectors in a sector of the reference current vector. During a switching period, the duty cycle of the vectors are calculated as follows:

$$\begin{cases} d_\alpha(\theta) = m\sin(\dfrac{\pi}{3} - \theta) \\ d_\beta(\theta) = m\sin(\theta) \\ d_0(\theta) = 1 - d_\alpha(\theta) - d_\beta(\theta) \end{cases} \tag{2}$$

where m is the modulation index, and $m \in [0,1]$; θ is the angle between I_{ref} and I_α ; and $d_\alpha(\theta)$, $d_\beta(\theta)$ and $d_0(\theta)$ are the duty cycles of I_α , I_β and I_0 , respectively. The average dc output voltage in one switching period can be calculated as [5]:

$$V_{\text{PN}} = 1.5 m V_{\text{im}} \cos\varphi_{\text{i}} \tag{3}$$

where V_{im} is the amplitude of the input phase voltage; and φ_{i} is the power factor angle of the main circuit.

When the grid side input voltage is unbalanced, the dc output voltage can be expressed as:

$$V_{\mathrm{PN}} = 1.5m(V_{\mathrm{im}} \pm \Delta V)\cos\varphi_{\mathrm{i}} \tag{4}$$

where ΔV denotes the amplitude variation of the ac supply.

From Eq. (4), it is indicated that V_{PN} is determined by the input voltage amplitude, modulation index and input power factor. Therefore, a desired output voltage can be maintained at a stable value with a unity IPF by adaptively changing the modulation index *m* under normal or non-normal conditions, such as a distorted input voltage.

III. Sliding Mode Control for DC Output Voltage

With the advantages of easier computation, simple structure, fast dynamic response, strong robustness and so on, SMC has recently been used in matrix rectifiers. However, SMC is a kind of special nonlinear feedback control that is reflected in the control of discontinuity, which results in a tremendous chattering. In addition, the reaching phase of SMC makes the robustness of a system decrease. In this section, a global sliding mode controller based on a hyperbolic tangent function has been applied to solve these problems.

A. Conventional Sliding Mode Control and Equivalent Sliding Mode Control

From Fig. 1 and Eq. (4), an equation for the state of the capacitor voltage and inductor current can be given as:

$$\begin{bmatrix} \dot{V}_0 \\ \dot{I}_{\mathrm{dc}} \end{bmatrix} = \begin{bmatrix} -\dfrac{1}{R_{\mathrm{L}}C_0} & \dfrac{1}{\mathrm{C}_0} \\ -\dfrac{1}{\mathrm{L}_0} & 0 \end{bmatrix} \begin{bmatrix} V_0 \\ I_{\mathrm{dc}} \end{bmatrix} + \begin{bmatrix} 0 \\ \dfrac{1}{L_0} \end{bmatrix} \left[1.5m(V_{\mathrm{im}} \pm \Delta V)\right] \tag{5}$$

Assume that the target voltage and output voltage are V_{ref} and V_0, respectively. If the feedback output voltage error variable $e_{\mathrm{V}} = V_{\mathrm{ref}} - V_0$ is defined, the sliding surface $S_1 = e_{\mathrm{V}} + c_1\dot{e}_{\mathrm{V}}$ is derived, and c_1 is the small positive sliding mode coefficient.

Then the control function of CSMC is as follows:

$$m = \begin{cases} 1, & S_1 > 0 \\ 0, & S_1 < 0 \end{cases} \tag{6}$$

Since its modulation index *m* switches between the minimum 0 and maximum 1, the dc output voltage has a violent chattering. Equivalent SMC can be used to slow down the switching value of *m*, and to weaken the chattering of the dc output voltage. When external disturbances and parameter variations are not considered in advance, suppose that there is a unity IPF. Then the equivalent control term of SMC can be obtained:

$$m_{\mathrm{ref}} = \frac{V_{\mathrm{ref}}}{1.5V_{\mathrm{im}}} \tag{7}$$

Hence, the control function of equivalent SMC is expressed as:

$$m = \begin{cases} m_{\mathrm{ref}} + \sigma, & S_1 > 0 \\ m_{\mathrm{ref}} - \sigma, & S_1 < 0 \end{cases} \tag{8}$$

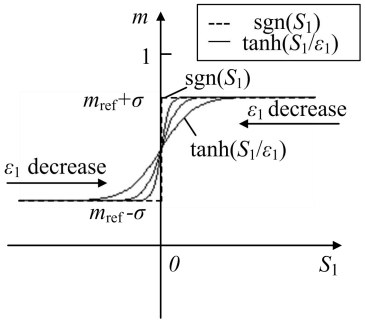

Fig. 3. Curves of *m* with different functions.

where σ is the value of the voltage anti-disturbance, which is the switching control term of equivalent SMC. Under normal circumstances, the grid side voltage unbalance factor standard is not more than ±4% [22]. However, in peak periods of electricity demand or late at night, voltage often exceed the standard. According to the range of the modulation index *m*, the value of the voltage anti-disturbance can be $\sigma \in [0.05,0.1]$.

The equivalent control term makes systems stay at the sliding surfaces, and the switch control term allows systems to slide on the surfaces. The switching term can guarantee the robustness of a system. However, the chattering of the sliding mode is generated by it. When the system robustness is ensured, in order to suppress the chattering of the sliding mode, the switching term is kept as small as possible. In other words, when the grid side voltage disturbance is larger, the voltage anti-disturbance is larger; and when the grid voltage disturbance is smaller, the voltage anti-disturbance is smaller.

However, these SMCs are based on the symbolic function, which is a discontinuous function. Applying a symbolic function cannot be adapted to change the value of the voltage anti-disturbance, and there is a large chattering.

B. Sliding Mode Control Based on a Hyperbolic Tangent Function

In order to further suppress the chattering, SMC can be replaced by a continuous hyperbolic tangent function. The control function of SMC based on a hyperbolic tangent function is as follows:

$$m = m_{\mathrm{ref}} + \tanh(S_1/\varepsilon_1)\sigma \tag{9}$$

where ε_1 is a small positive constant, which determines the speed of the inflection point. Since $\tanh(S_1) \in [-1,1]$, then $m \in [m_{\mathrm{ref}} - \sigma, m_{\mathrm{ref}} + \sigma]$, and the value of S_1 changes with external disturbances and parameter uncertainties, as well as the modulation index *m*. As shown in Fig. 3, there are change curves of *m* when using various control functions for SMC.

From Fig. 3, it should noted that ε_1 approaches 0, the hyperbolic tangent function is equivalent to the symbolic function, which has a serious influence on the continuity of the control function, and the sliding mode chattering becomes more obvious if ε_1 is decreased from a set-point.

Due to the reachability and existence of SMC, the following must be satisfied:

$$S_1 \dot{S}_1 < 0 \tag{10}$$

where $S_1 = e_V + c_1 \dot{e}_V$, while the target voltage V_{ref} is a constant, $\dot{V}_{ref} = 0$. Then $\dot{e}_V = -\dot{V}_0$. Thus, substituting Eq. (5) into Eq. (10) yields:

$$\begin{aligned} S_1 \dot{S}_1 &= S_1 \left[(V_{ref} - V_0) - \frac{c_1}{C_0}(I_{dc} - \frac{V_0}{R_L}) \right] \\ &= S_1 \left[\dot{V}_0 (\frac{c_1}{R_L C_0} - 1) - \frac{c_1}{C_0} \dot{I}_{dc}) \right] \end{aligned} \tag{11}$$

When c_1 is small enough, and rated load $R_L = 50\Omega$, there is $(\frac{c_1}{R_L C_0} - 1) \approx -1$. Consequently, substituting Eq. (5), (7) and (9) into Eq. (11) results in:

$$S_1 \dot{S}_1 = -\frac{S_1}{C_0} \left[(I_{dc} - \frac{V_0}{R_L}) + \frac{c_1}{L_0} \left(1.5m(V_{im} \pm \Delta V) - V_0\right) \right] < 0 \tag{12}$$

where:

$$\begin{aligned} &1.5m(V_{im} \pm \Delta V) = 1.5[m_{ref} + \tanh(S_1/\varepsilon_1)\sigma](V_{im} \pm \Delta V) = \\ &V_{ref} + 1.5V_{im} \tanh(S_1/\varepsilon_1)\sigma \pm \frac{V_{ref}}{V_{im}} \Delta V \pm 1.5\Delta V \tanh(S_1/\varepsilon_1)\sigma \end{aligned} \tag{13}$$

From [23], for any arbitrary $S_1 \in R$, there is a constant $\varepsilon_1 > 0$, and the following inequality is established:

$$0 \le |S_1| - S_1 \tanh(S_1/\varepsilon_1) \le \mu\varepsilon_1 \tag{14}$$

where $\mu = e^{-(\mu+1)}$. Therefore, $\mu = 0.2785$. Then Eq. (14) can be transformed as:

$$\begin{cases} \tanh(S_1/\varepsilon_1)\sigma \ge \dfrac{\sigma|S_1| - \sigma\mu\varepsilon_1}{S_1} \ge 0, & S_1 > 0 \\ \tanh(S_1/\varepsilon_1)\sigma \le \dfrac{\sigma|S_1| - \sigma\mu\varepsilon_1}{S_1} \le 0, & S_1 < 0 \end{cases} \tag{15}$$

From here on, there are separated into two parts to discuss whether Eq. (12) is satisfied or not.

1) If $S_1 > 0 \Rightarrow S_1 \approx (V_{ref} - V_0) > 0$ *.:* In this switching cycle, because the main circuit charges the filter capacitor and supplies power to the load, there is $(I_{dc} - V_0/R_L) > 0$. At the same time, the inequality $[1.5V_{im} \tanh(S_1/\varepsilon_1)\sigma \pm \frac{V_{ref}}{V_{im}} \Delta V \pm 1.5\Delta V \tanh(S_1/\varepsilon_1)\sigma] \ge 0$ should be established, where only $\tanh(S_1/\varepsilon_1)\sigma \ge \mp \frac{V_{ref}\Delta V}{1.5V_{im}(V_{im} \pm \Delta V)}$ holds. Because all positive numbers are bigger than negative numbers, $\tanh(S_1/\varepsilon_1)\sigma \ge \frac{V_{ref}\Delta V}{1.5V_{im}(V_{im} \pm \Delta V)}$. As previously mentioned, in the peak period or late at night, grid side voltage fluctuations are often excessive. In order to make systems have better robustness, let $V_{im} = 10\Delta V$ (the value can be self-set depending on the actual situation). Then $\tan(S_1/\varepsilon_1)\sigma \ge \frac{V_{ref}}{13.5V_{im}}$. From Eq. (15), and if $\frac{\sigma|S_1| - \sigma\mu\varepsilon_1}{S_1} \ge \frac{V_{ref}}{13.5V_{im}}$ exists, $\tanh(S_1/\varepsilon_1)\sigma \ge \frac{V_{ref}}{13.5V_{im}}$ is established. Therefore, the voltage anti-disturbance $\sigma \ge \frac{S_1}{|S_1| - \mu\varepsilon_1} \cdot \frac{V_{ref}}{13.5V_{im}}$ is fulfilled, the inequality $[1.5V_{im} \tanh(S_1/\varepsilon_1)\sigma \pm \frac{V_{ref}}{V_{im}} \Delta V \pm 1.5\Delta V \tanh(S_1/\varepsilon_1)\sigma] \ge 0$ holds. This means that $S_1 \dot{S}_1 < 0$.

2) If $S_1 < 0 \Rightarrow S_1 \approx (V_{ref} - V_0) < 0$ *.:* Since both the filter capacitor and the inductor supply power to the load, in this switching cycle, $(I_{dc} - V_0/R_L) < 0$. Similarly, the inequality $[1.5V_{im} \tanh(S_1/\varepsilon_1)\sigma \pm \frac{V_{ref}}{V_{im}} \Delta V \pm 1.5\Delta V \tanh(S_1/\varepsilon_1)\sigma] \le 0$ should be established, where only $\tanh(S_1/\varepsilon_1)\sigma \le \mp \frac{V_{ref}\Delta V}{1.5V_{im}(V_{im} \pm \Delta V)}$ exists. Since all negative numbers are smaller than positive numbers, $\tanh(S_1/\varepsilon_1)\sigma \le -\frac{V_{ref}\Delta V}{1.5V_{im}(V_{im} \pm \Delta V)}$. As mentioned above, in order to make the system more robust, $V_{im} = 10\Delta V$. Then $\tanh(S_1/\varepsilon_1)\sigma \le -\frac{V_{ref}}{13.5V_{im}}$. From (15), if $\frac{\sigma|S_1| - \sigma\mu\varepsilon_1}{S_1} \le -\frac{V_{ref}}{13.5V_{im}}$, $\tanh(S_1/\varepsilon_1)\sigma \le -\frac{V_{ref}}{13.5V_{im}}$ will be established. Therefore, the voltage anti-disturbance $\sigma \ge \frac{-S_1}{|S_1| - \mu\varepsilon_1} \cdot \frac{V_{ref}}{13.5V_{im}}$ is assured, and the inequality $[1.5V_{im} \tanh(S_1/\varepsilon_1)\sigma \pm \frac{V_{ref}}{V_{im}} \Delta V \pm 1.5\Delta V \tanh(S_1/\varepsilon_1)\sigma] \le 0$ holds, which means that $S_1 \dot{S}_1 < 0$.

In conclusion, the voltage anti-disturbance is as $\sigma \ge \frac{|S_1|}{|S_1| - \mu\varepsilon_1} \cdot \frac{V_{ref}}{13.5V_{im}}$. Since $\mu = 0.2785$ is a fixed invariant constant, as long as ε_1 is small enough, the right end of the inequality converges to $\lim_{\varepsilon \to 0} (\frac{|S_1|}{|S_1| - \mu\varepsilon_1} \cdot \frac{V_{ref}}{13.5V_{im}}) = \frac{V_{ref}}{13.5V_{im}}$. If and only if the given inequality condition $\sigma \ge \frac{V_{ref}}{13.5V_{im}}$ is satisfied, the SMC for the dc output voltage of a MR has good robustness.

As a constant to determine the speed of the inflection point of $m = m_{ref} + \tanh(S_1/\varepsilon_1)\sigma$, from Fig. 3, it should be noted that as ε_1 approaches 0, $\tanh(S_1/\varepsilon_1) \approx \mathrm{sgn}(S_1)$; and that as ε_1 approaches infinity, $\tanh(S_1/\varepsilon_1) \approx 0$. Then when ε_1 is too small, although the robustness is better, the ability of the voltage anti-disturbance self-regulation is too weak, and the dc

output voltage chattering is more obvious. When ε_1 is too large, while the chattering suppression effect is superior, the robustness is poor. Therefore, ε_1 should be adjusted appropriately to ensure both robustness and chattering reduction.

According to the principles above, a rough value of ε_1 is first selected. Then increasing or decreasing ε_1 in several tests can finally obtain an appropriate value of $\varepsilon_1 = 1$, which ensures better robustness and superior ability in terms of chattering suppression.

C. Global sliding Mode Control

GSMC is achieved by eliminating the sliding mode reaching phase. This guarantees that the system states are in the sliding mode from a given initial state to enhance the robustness of the overall system. For this, it is defined that the sliding surface is equal to zero to design a novel global sliding mode switching function as:

$$S_{G1} = S_1 - f(t) \tag{16}$$

where the term $f(t)$ is a forcing function, which is a desired trajectory function for the system. In addition, the conditions of the forcing function $f(t)$ should be satisfied that:

1) $f(0) = S_1(0)$.

2) $t \to \infty$, $f(t) \to 0$.

3) $\dot{f}(t)$ exits and is bounded.

where $S_1(0) = S_1(t = 0)$. Furthermore, condition (1) means that the system state is initially kept at the sliding surface, condition (2) guarantees the asymptotic stability of the closed-loop system, and condition (3) is satisfied for the reachability and existence of the SMC [24].

Hence, the forcing function $f(t)$ can be prescribed as:

$$f(t) = f(0)e^{-\lambda t} \tag{17}$$

where $\lambda > 0$, and $f(0)$ is the initial value of S_1. Then, the function $f(t)$ can be discretized as:

$$f(n+1) = f(n)e^{-\lambda} \tag{18}$$

and:

$$f(n) = f(0)e^{-\lambda n} \tag{19}$$

According to condition (2), when $t \to \infty$, $f(0)$ finally decays to 0, and the constant λ determine its decay rate. When the value of λ is too large, the decay rate is too fast, and GSMC cannot play the role of eliminating the sliding mode reaching phase. When λ is too small, the decay rate is too slow, and the value of $f(0)$ cannot be attenuated to 0. This means that condition (2) is not satisfied and the system stability becomes more difficult, resulting in output voltage distortion.

For a comprehensive consideration, in order to ensure that the value $f(0)$ decays to 1% of the original value or less after seven switching periods, $\lambda \approx 0.66$.

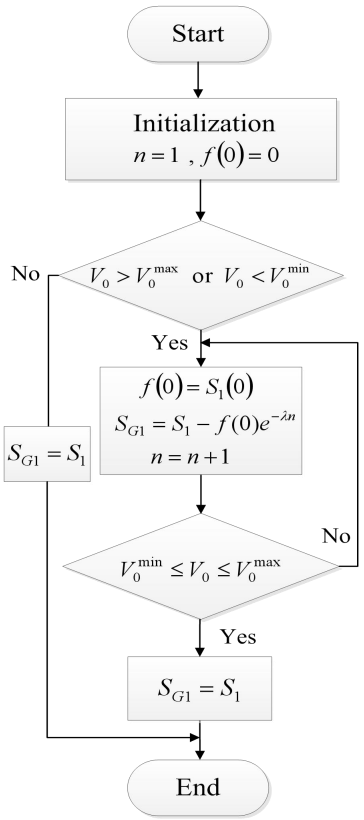

Fig. 4. Flow chart of global SMC.

The focus of GSMC is to design an appropriate global switching function, and the key is the determination of the steady state and transient state. Therefore, the maximum and minimum theoretical value of the dc output voltage for a MR can be used as a judgment criterion in this paper as follows:

$$\begin{cases} V_0^{\max} = 1.5V_{\text{im}}(m_{\text{ref}} + \sigma) \\ V_0^{\min} = 1.5V_{\text{im}}(m_{\text{ref}} - \sigma) \end{cases} \tag{20}$$

When $V_0 > V_0^{\max}$ or $V_0 < V_0^{\min}$, the MR works in the transient state. Otherwise, it works in the steady state.

A GSMC flow chart is shown in Fig. 4, and the details are as follows. First, detect the dc output voltage V_0 to determine whether or not it satisfies $V_0 > V_0^{\max}$ or $V_0 < V_0^{\min}$. If not, the MR works in the steady state and does not need to deal with the switching function. If it does, the MR works in the transient state. The current value of $S_1(0)$ is assigned to $f(0)$. Then the system is in the sliding state until the end of the transient state.

The role of the second judgment frame is to judge whether the system is in the steady state. In addition, the global switching function is changed to the initial switching function if the condition is met.

IV. Compensation Strategy for the IPF

Unfortunately, the above-mentioned analysis for a MR is

conducted with a unity IPF, and the IPF should be decreased due to the existence of an input filter. Therefore, a SMC compensation strategy is proposed in this section.

A. DQ Equivalent Model of a MR

As a multivariable, nonlinear, strong coupling, parameter time-changing complex system, the modeling and analysis of a MR is often more difficult. A DQ transformation model for a MR is given in Fig. 5 to solve the problem.

To simplify the circuit, assuming that the phase between the d-axis and the q-axis φ is equal to the phase between the input voltage and current φ_i. With a short-circuit of the inductors and an open-circuit of the capacitors, the dc analysis circuit of a MR in steady state is simplified in Fig. 6, and the relationship between the voltage and current at the steady state operating point are as:

$$\begin{cases} u_{sd} = \sqrt{\frac{3}{2}}\frac{3\omega L_i m V_{im}\cos\varphi_i}{2R_L(1-\omega^2 C_i L_i)^2} - \sqrt{\frac{3}{2}}\frac{V_{im}\sin\varphi_i}{1-\omega^2 C_i L_i} \\ u_{sq} = \sqrt{\frac{3}{2}}\frac{V_{im}\cos\varphi_i}{1-\omega^2 C_i L_i} \\ i_{sq} = \sqrt{\frac{3}{2}}\frac{3m^2 V_{im}\cos\varphi_i}{2R_L(1-\omega^2 C_i L_i)^2} - \sqrt{\frac{3}{2}}\frac{\omega C_i V_{im}\sin\varphi_i}{1-\omega^2 C_i L_i} \\ i_{sd} = -\sqrt{\frac{3}{2}}\frac{\omega C_i V_{im}\cos\varphi_i}{1-\omega^2 C_i L_i} \end{cases} \quad (21)$$

where u_{sd} and u_{sq} are the d-axis and q-axis input voltage, and i_{sd} and i_{sq} are the d-axis and q-axis input current, respectively.

Consequently, the input active power and reactive power are expressed as follows:

$$\begin{cases} P = u_{sd}i_{sd} + u_{sq}i_{sq} \\ \quad = \dfrac{9V_{im}^2 m^2\cos^2\varphi_i}{4R_L(1-\omega^2 C_i L_i)^2} \\ Q = u_{sq}i_{sd} - u_{sd}i_{sq} \\ \quad = \dfrac{3V_{im}^2}{2(1-\omega^2 C_i L_i)}\left[\dfrac{3m^2\sin(2\varphi_i)}{4R_L(1-\omega^2 C_i L_i)} - \omega C_i\right] \end{cases} \quad (22)$$

When $|\varphi_i| < \pi/6$ and $\omega C_i L_i << 1$, it follows that $\sin(2\varphi_i) \approx 2\varphi_i$ and $(1-\omega C_i L_i) \approx 1$. To achieve a unity IPF, it is indicated that the input reactive power $Q = 0$. This means that:

$$\varphi_i \approx \frac{2\omega R_L C_i}{3m^2} \quad (23)$$

where φ_i is the compensation angle, and φ_i varies inversely with m^2. This means that a larger modulation index m would need a smaller compensation angle φ_i with the other conditions being kept constant.

In order to guarantee the high transmission ratio of a MR, the maximum compensation angle is set as $\varphi_{imax} = \pi/6$, and the target compensation angle φ_{ref} can be expressed as:

$$\varphi_{ref} = \min\left(\frac{2\omega R_L C_i}{3m^2}, \frac{\pi}{6}\right) \quad (24)$$

The change curve of φ_{ref} is shown in Fig. 7. When the value of m is less than the turning point, the target compensation angle is kept in a constant state. However, when the value of m is greater than the turning point, the target compensation angle is decreased with the increase of m.

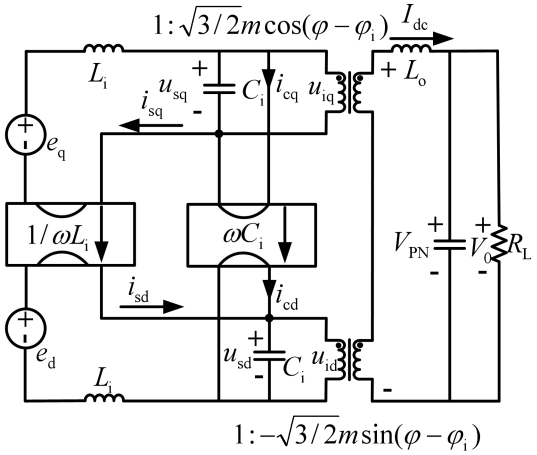

Fig. 5. DQ transformed equivalent circuit of a MR.

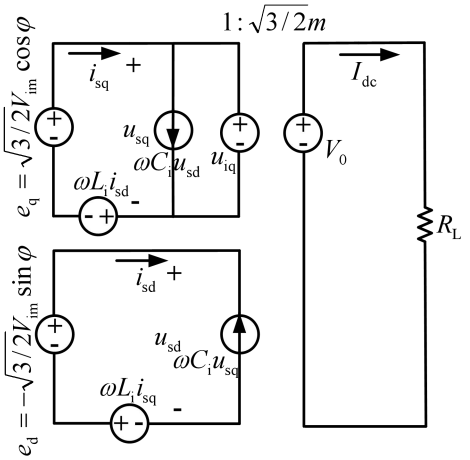

Fig. 6. DQ transformed simplified equivalent circuit of a MR in the steady state with $\varphi = \varphi_i$.

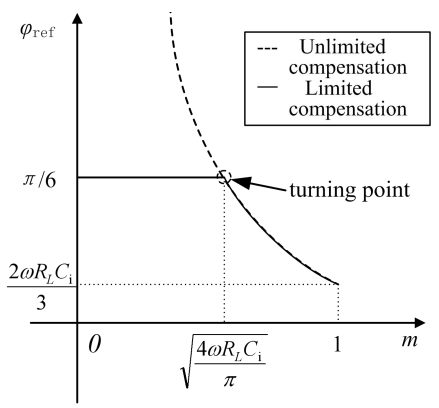

Fig. 7. Change curve of φ_{ref}.

B. Sliding Mode Control Compensation Algorithms for the Input Power Factor

However, the compensation angle φ_i changes slightly with modeling parameter variations and is not a certain constant.

Thus, a SMC is applied to ensure better dynamic compensation characteristics. The sliding mode switching function is defined as:

$$S_2 = Q + c_2 \dot{Q} \tag{25}$$

where c_2 is a positive constant. Then the control function is:

$$\varphi_i = \begin{cases} \varphi_{ref} + \delta, & S_2 > 0 \\ \varphi_{ref} - \delta, & S_2 < 0 \end{cases} \tag{26}$$

where δ is the disturbance resist factor. Similarly, Eq. (26) can be transferred by a continuous hyperbolic tangent function as follows:

$$\varphi_i = \varphi_{ref} + \tan(S_2 / \varepsilon_2)\delta \tag{27}$$

SMC is in local reachability only if the following condition is met:

$$S_2 \dot{S}_2 < 0 \tag{28}$$

If c_2 is small enough, Eq. (28) can be simplified as:

$$S_2 \dot{S}_2 = (Q + c_2 \dot{Q})(\dot{Q} + c_2 \ddot{Q}) \approx Q \dot{Q} \tag{29}$$

From Eq. (22), the change rate of Q in one switching period is calculated as:

$$\dot{Q} = \frac{9 V_{im}^2 m^2}{4 R_L} \dot{\varphi}_i \tag{30}$$

where $\dot{\varphi}_i$ is also the change rate of φ_i in one switching period.

1). If $S_2 > 0 \Rightarrow Q > 0$. From Eq. (27), $\tan(S_2^k / \varepsilon_2)\delta > 0$ in the current cycle, and $\tan(S_2^{k+1} / \varepsilon_2)\delta < 0$ in the following cycle. Then:

$$\begin{aligned} \dot{\varphi}_i &= (\varphi_i^{k+1} - \varphi_i^k) f_s \\ &= [\tan(S_2^{k+1} / \varepsilon_2) - \tan(S_2^k / \varepsilon_2)] \delta f_s < 0 \end{aligned} \tag{31}$$

where f_s is the switching frequency.

By substituting Eq. (30) and Eq. (31) into Eq. (29), it is possible to hold Eq. (28), which means that the sliding mode exists.

2). If $S_2 < 0 \Rightarrow Q < 0$. From Eq. (27), $\tan(S_2^k / \varepsilon_2)\delta < 0$ in the current cycle, and $\tan(S_2^{k+1} / \varepsilon_2)\delta > 0$ in following cycle. Then:

$$\begin{aligned} \dot{\varphi}_i &= (\varphi_i^{k+1} - \varphi_i^k) f_s \\ &= [\tan(S_2^{k+1} / \varepsilon_2) - \tan(S_2^k / \varepsilon_2)] \delta f_s > 0 \end{aligned} \tag{32}$$

By substituting Eq. (30) and Eq. (32) into Eq. (29), it is possible to hold Eq. (28), which means that the sliding mode exists.

In conclusion, the sliding mode is established in any case. In addition, a diagram of the control system for a MR is shown in Fig. 8.

V. Simulation and Experiment Results

To further validate the correctness and effectiveness of the proposed control strategy, a detailed simulation and an experimental prototype of a MR with a resistive load were built and presented in this section. The parameters are the same as those in Table I.

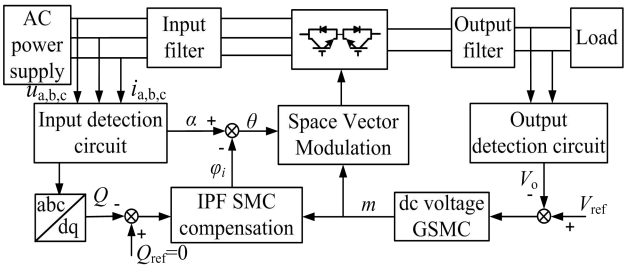

Fig. 8. Diagram of a control system for a MR.

TABLE I
Parameters of the Experimental Prototype

Parameters	Value
Input voltage U_i / V	50
Input frequency f_i / Hz	50
Inductor of input filter L_i / mH	2
Capacitor of input filter C_i / μF	20
Damping resistance of input filter R_i / Ω	15
Inductor of output filter L_0 / mH	5
Capacitor of output filter C_0 / μF	33
Load resistance R_L / Ω	50
Sampling frequency f_s / kHz	10
Voltage anti-disturbance σ	0.1
Disturbance resist factor δ	0.05
Sliding mode coefficient c_1 ,c_2	6×10^{-5} , 8×10^{-6}
ε_1 , ε_2	1,1

A. Simulation and Analysis

A small-scale simulation model was built in the MATLAB/SIMULINK platform and three comparative simulations were carried out. 1) A three phase balanced input voltage using SVM with or without GSMC and compensation. 2) GSMC with a different parameter for the constant λ. 3) A three phase unbalanced input voltage using SVM with or without GSMC and compensation. The target voltage is set to change from 80V to 50V.

Fig. 9 shows simulation results using the same circuit parameters with or without GSMC and compensation under a balanced power supply. When applying SVM without compensation, as shown in Fig. 9(a), the dynamic performance is poor, and low the frequency fluctuation are more obvious. In addition, from Eq. (23), a higher dc output voltage corresponds to a larger modulation index m, as well as a smaller compensation angle, then $\Delta t1 < \Delta t2$.

Furthermore, compared with the conventional SVM, no matter what the output voltage is, applying GSMC with compensation achieves a quicker response and a ripple-free voltage with a

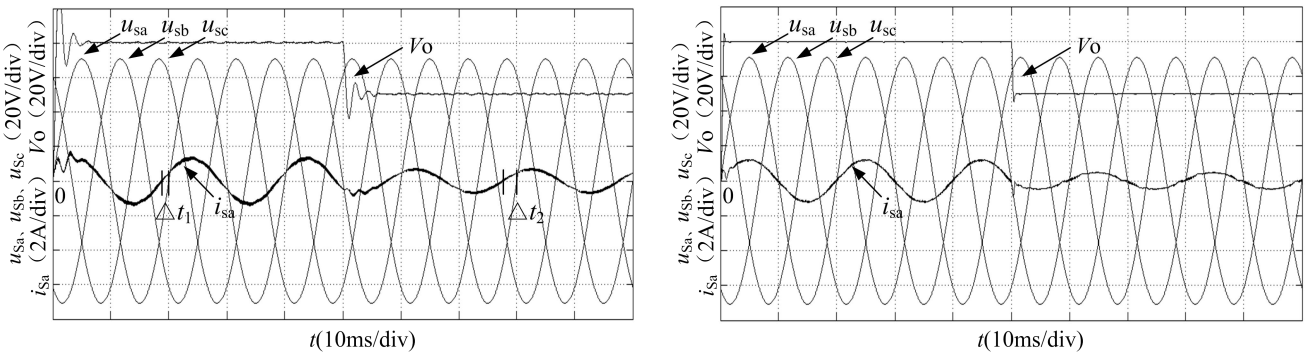

Fig. 9. Simulation waveforms with a balanced input voltage: (a) SVM without compensation, (b) GSMC with compensation.

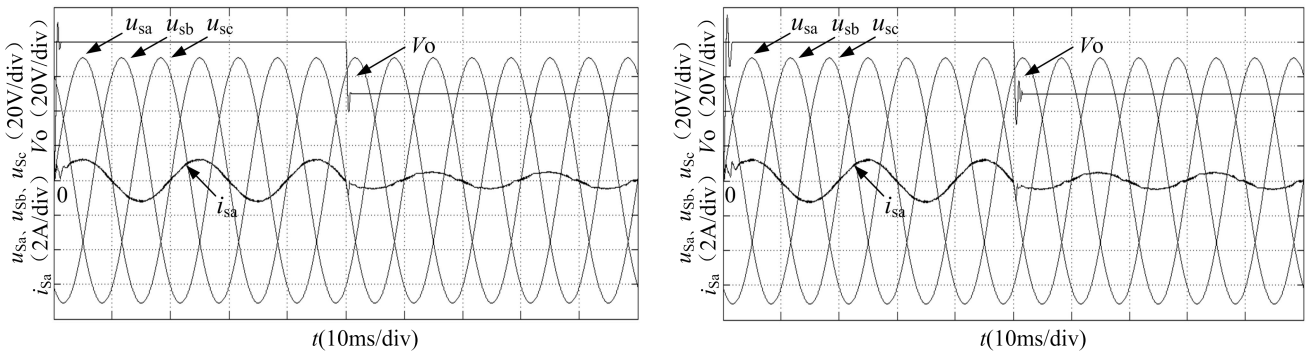

Fig. 10. Simulation waveforms with a different parameter of the constant λ: (a) $\lambda = 6.6$, (b) $\lambda = 0.066$.

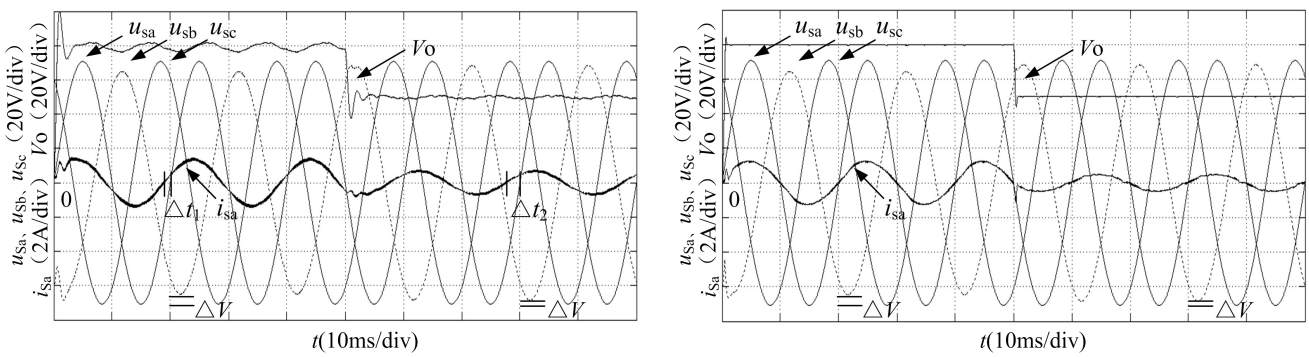

Fig.11. Simulation waveforms with an unbalanced input voltage: (a) SVM without compensation, (b) GSMC with compensation.

near unity IPF, as shown in Fig. 9(b).

Fig. 10 shows simulation results with a different value of the constant λ. From Fig. 10(a), the value of the constant $\lambda = 6.6$ is too large, the decay rate is too fast, and the GSMC cannot play the role of eliminating the sliding mode reaching phase, which is a larger overshoot. In Fig. 10(b), the value of the constant $\lambda = 0.066$ is too small, the decay rate is too slow, the value of $f(0)$ cannot be attenuated to 0 in the end. This means that the system is more difficult to stabilize, resulting in output voltage distortion. A comparison of the simulation data and the analysis results shows a good consistency.

When the input voltage is unbalanced (adding a resistor R=5Ω in series with B phase), as in Fig. 11(a), because SVM is an open-loop control, there is a tremendous ripple. However, applying GSMC with compensation can effectively restrain the output voltage fluctuations and provide a ripple-free output voltage with a near unity IPF, as shown in Fig. 11(b).

B. Experiment and Analysis

A laboratory prototype was realized for hardware verification in Fig. 12, and six comparative experiments were carried out. 1) A three phase balanced input voltage using conventional SVM without compensation. 2) A three phase balanced input voltage using various SMCs with compensation. 3) SMC based on a hyperbolic tangent function with different values of ε_1. 4) GSMC based on a hyperbolic tangent

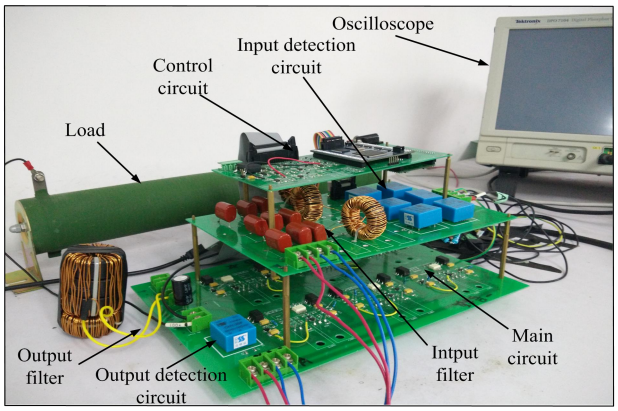

Fig. 12. Physical map of the prototype.

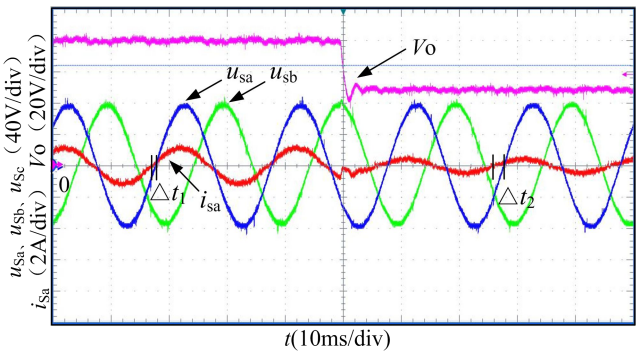

Fig. 13. Experimental waveforms of using SVM without compensation under a balanced input voltage.

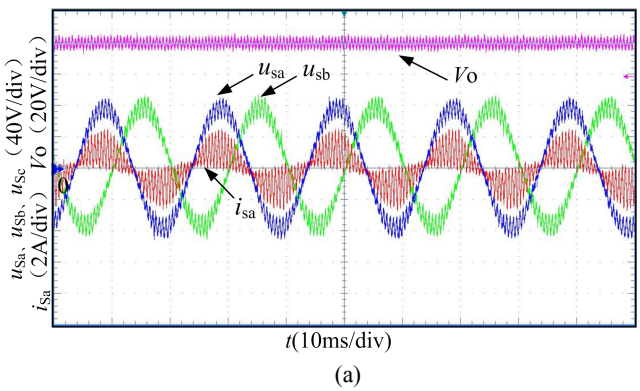

(a)

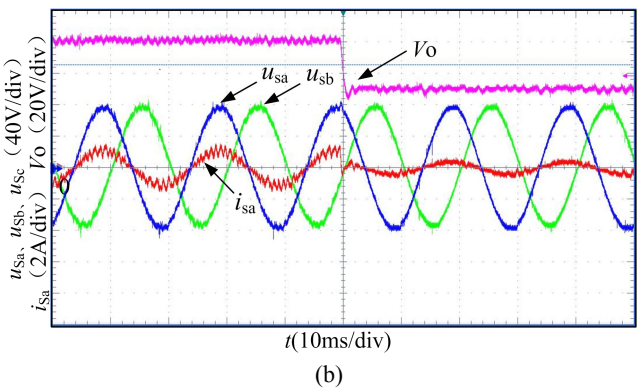

(b)

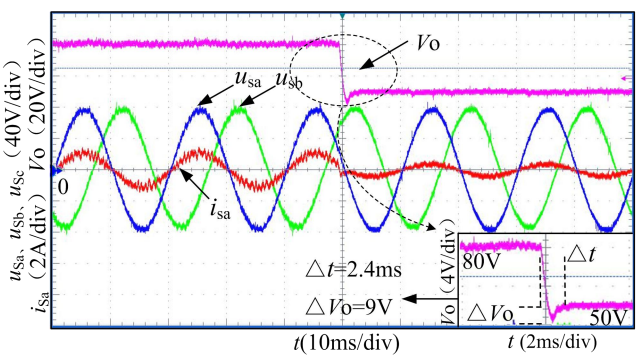

(c)

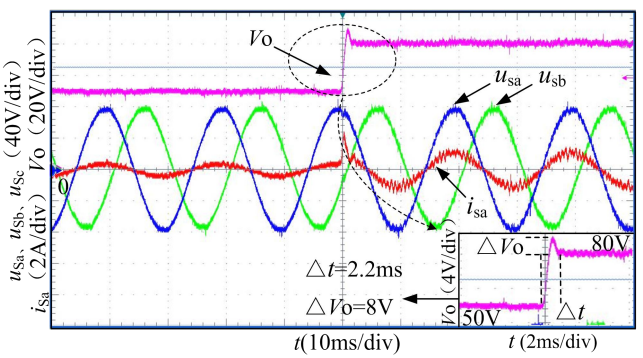

(d)

Fig. 14. Experimental waveforms with a balanced input voltage: (a) conventional SMC with compensation, (b) equivalent SMC with compensation, (c) and (d) SMC based on a hyperbolic tangent function with compensation: the dc output target voltage changes between 50V and 80V.

function. 5) A three phase unbalanced input voltage using conventional SVM without compensation. 6) A three phase unbalanced input voltage using various SMCs with compensation. The experiment results for these experiments are shown in Fig. 13 to Fig. 18.

As shown in Fig. 13, using SVM can result in a desired output voltage. However, when using SVM without any control strategy or compensation, there is a low-quality waveform and a decreasing IPF. Like the simulation results, in the case of low output voltage conditions, the IPF is significantly decreased ($\triangle t_1 < \triangle t_2$).

According to Fig. 14(a), the conventional SMC with compensation can obtain a stable dc output voltage with a near unity IPF. However, there is a violent chattering. When equivalent SMC is adopted, the chattering can be greatly reduced, as shown in Fig. 14(b). However, above methods are based on the discontinuous function of SMC. When compared to SMC based on a continuous hyperbolic tangent function in Fig. 14(c) and Fig. 14(d), the chattering is more obvious. It can be seen that SMC can effectively restrain the chattering and improve the quality of waveforms by using a continuous function instead of a discontinuous function.

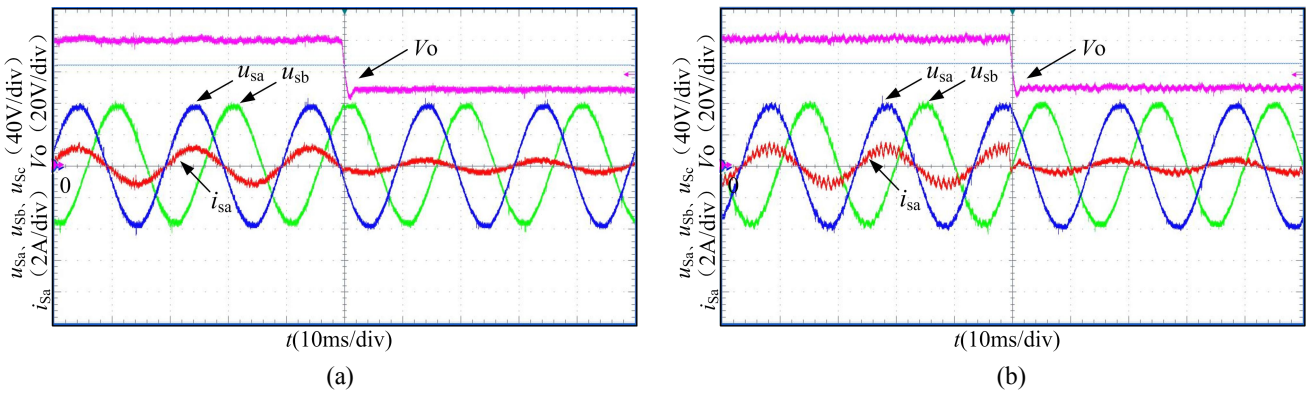

Fig. 15. Experimental results of SMC based on a hyperbolic tangent function with different values of ε_1: (a) $\varepsilon_1 = 10$, (b) $\varepsilon_1 = 0.1$.

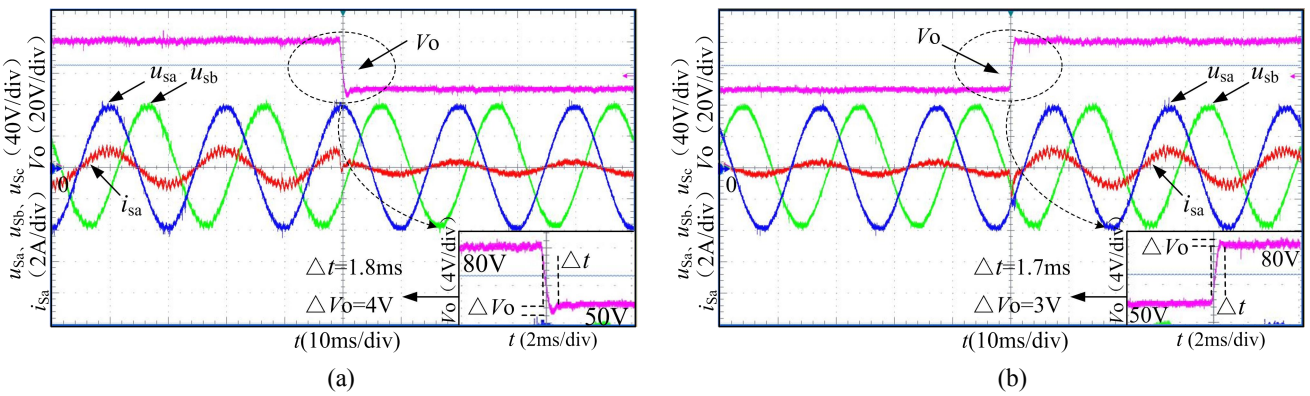

Fig. 16. Experimental results of GSMC based on a hyperbolic tangent function when the dc output target voltage changes: (a) 80V to 50V, (b) 50V to 80V.

A desired dc output voltage can be obtained when $\varepsilon_1 = 10$ and $\varepsilon_1 = 0.1$ (when the value of ε_1 is larger or smaller). However, as shown in Fig. 15(a), a larger value of ε_1 makes the overshoot become larger and the robustness poor, which increases the output voltage fluctuations. In Fig. 15(b), while the system reduces the overshoot and improves robustness through a smaller value of ε, there is an obvious chattering. It is clear that the experimental results coincide well with the theoretical analysis mentioned above.

When the target voltage changes from 80V to 50V, as shown in to Fig. 14(c), using SMC based on a hyperbolic tangent function, the dynamic response time and output voltage overshoot are 2.4ms and 9V. Under the same conditions, using GSMC based on a hyperbolic tangent function, the dynamic response time and output voltage overshoot are 1.8ms and 4V, as shown in Fig. 16(a). This means that there is both a 25% and 55.6% reduction in the dynamic response time and in the output voltage overshoot, respectively.

In Fig. 14(d) and Fig. 16(b), when the target voltage changes from 50V to 80V, the dynamic response time is shortened by about 22.7% from 2.2ms in the SMC to 1.7ms in the GSMC. At the same time, the output voltage overshoot has also been decreased by 62.5% between 8V in the SMC to 3V in the GSMC.

Compared with SMC, GSMC has a smaller overshoot and better robustness.

When the three phase input voltage is unbalanced (adding a resistor R=5Ω in series with the B phase), using SVM without any control strategy or compensation, the dc output voltage has a tremendous ripple and the IPF is decreased, as shown in Fig. 17(a). However, the output voltage fluctuation can be eliminated and a near unity IPF can be achieved when the equivalent SMC with compensation is adopted, as shown in Fig. 17(b). In the case of the same parameters, using SMC based on a hyperbolic tangent function in Fig. 17(c) and Fig. 17(d) can eliminate the fluctuation of the dc output voltage with a near unity IPF, and effectively restrain the chattering. Thus, it possesses a superior advantage when compared to the others.

In addition, when the target voltage changes from 80V to 50V under an unbalanced input voltage, as shown in Fig. 17(c) and Fig. 18(a), the dynamic response time is shortened by about 14.3% from 2.1ms in the SMC to 1.8ms in the GSMC, while the overshoot is decreased by 42.9% from 7V in the SMC to 4V in the GSMC. Furthermore, when the target voltage changes from 50V to 80V, as shown in Fig. 17(d) and Fig. 18(b), the dynamic response time is shortened by about 18.2% from 2.2ms in the SMC to 1.8ms in the GSMC, while the overshoot is decreased by 55.6% from 9V in the SMC to

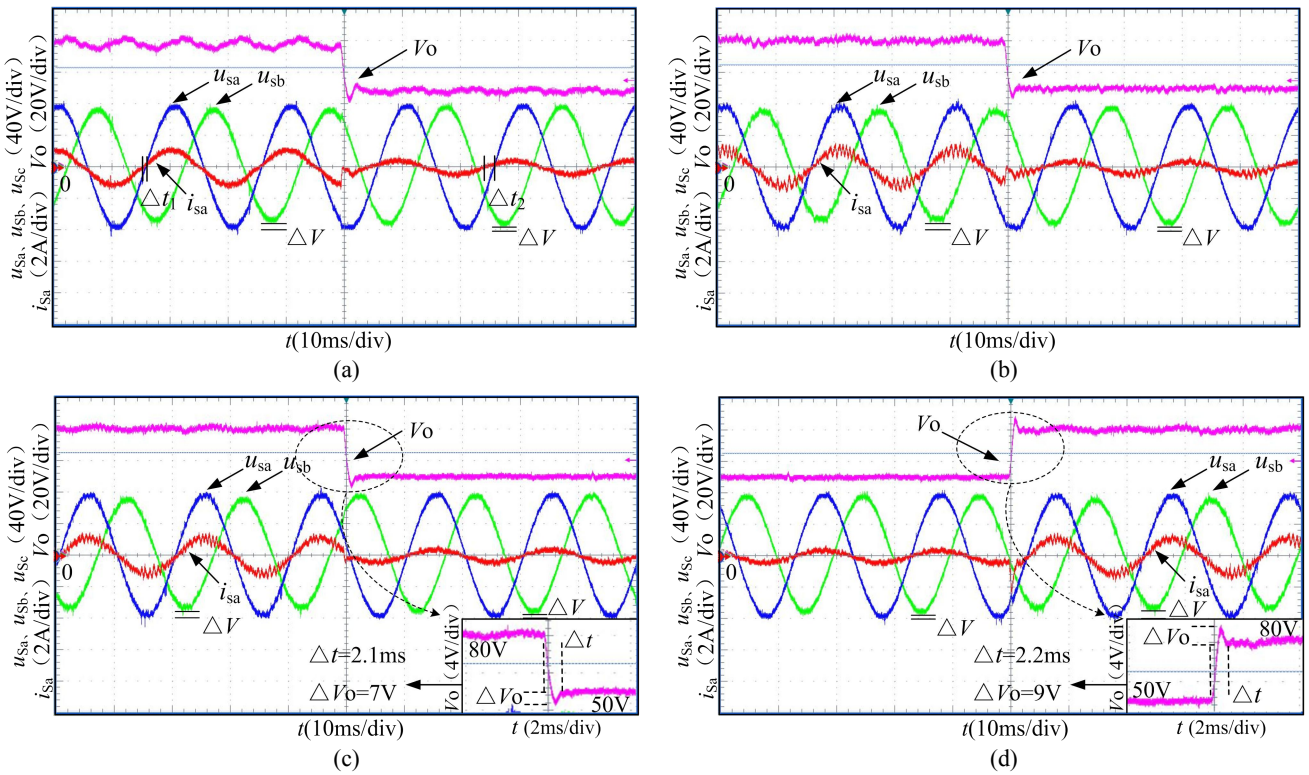

Fig. 17. Experimental results with an unbalance input voltage: (a) SVM without a control strategy or compensation, (b) equivalent SMC with compensation, (c) and (d) SMC based on a hyperbolic tangent function with compensation: the target voltage changes between 50V and 80V.

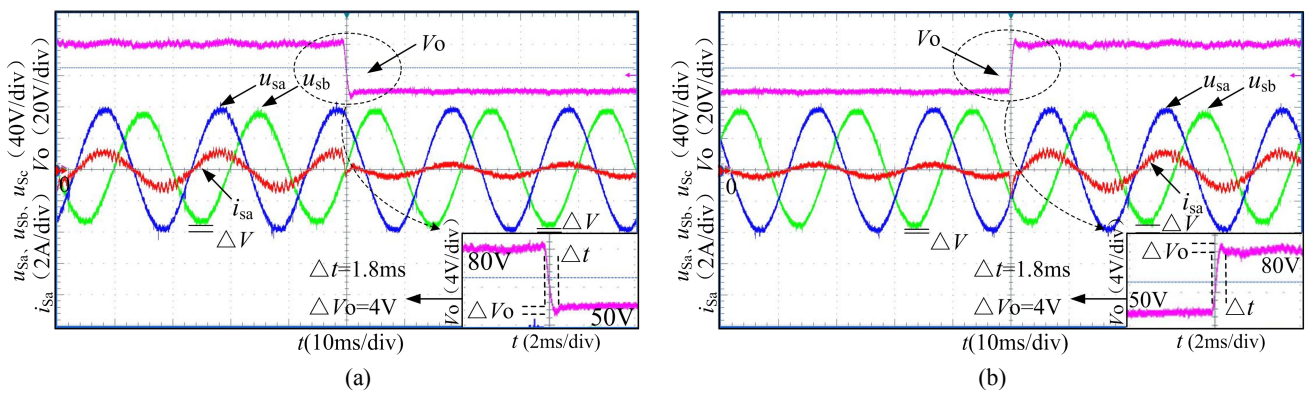

Fig. 18. Experimental results of GSMC based on a hyperbolic tangent function with an unbalance input voltage when the target voltage changes: (a) 80V to 50V, (b) 50V to 80V.

4V in the GSMC.

This means that GSMC is designed for better transient state response in the case of an unbalanced input voltage.

VI. Conclusions

In SMC for matrix rectifiers, a novel control strategy for GSMC based on a hyperbolic tangent function with IPF compensation has been proposed in this paper. In comparison with CSMC based on a discontinuous symbol function without compensation, the superior features of the proposed strategy are as follows:

1) Not redesigning the switching table makes the calculation easier to implement.

2) The output voltage chattering suppression effect is better by applying a smooth continuous hyperbolic tangent function.

3) Enhanced transient performance is obtained since the GSMC is adopted, which means that the system should be more robust in the whole process.

4) A unity IPF can be achieved accurately with a quicker response owning to the SMC compensation.

The above advantages are realized even if the input voltage

is distorted. Simulations and experimental results verify the correctness and effectiveness of the proposed SMC strategy. Furthermore, the proposed control strategy can be applied to other power converters, and it has great practical value.

ACKNOWLEDGMENT

This work was supported in part by the Frontier and Key Technological Innovation Special Foundation of Guangdong Province (Major Science and Technology Project), China, Grant 2016B090912006.

REFERENCES

[1] D. G. Holmes, and T. A. Lipo, "Implementation of a controlled rectifier using AC-AC matrix converter theory," *IEEE Trans. Power Electron*., Vol.7, No. 1, pp. 240-250, Jan. 1992.

[2] P. W. Wheeler, J. Rodriguez, J. C. Clare, L. Empringham, and A.Weinstein, "Matrix converter: A technology review," *IEEE Trans. Ind. Electron*., Vol. 49, No. 2, pp.276-288, Apr. 2002.

[3] R. Metidji, B. Metidji, and B. Mendil, "Design and implementation of a unity power factor fuzzy battery charger using an ultrasparse matrix rectifier," *IEEE Trans. Power Electron.*, Vol. 28, No. 5, pp.2269-2276, May 2013.

[4] M. Su, H. Wang, Y. Sun, J. Yang, W.J. Xiong, and Y. L. Liu, "AC/DC matrix converter with an optimized modulation strategy for V2G applications," *IEEE Trans. Power Electron.*, Vol. 28, No. 12, pp.5736-5745, Feb. 2013.

[5] X. Liu, Q. F. Zhang, D. L. Hou, and S. Y. Sun, "Improved space vector modulation strategy for AC-DC matrix converters," *Journal of Power Electronics*, Vol. 13, No. 4, pp.647-655, Apr. 2013.

[6] F. Blaabjerg, D. Casadei, C. Klumpner, M. Matteini, and C. Klumpner, "Comparison of two current modulation strategies for matrix converters under unbalanced input voltage conditions," *IEEE Trans. Ind. Electron.*, Vol. 49, No. 2, pp.289-296, Apr. 2002.

[7] H. M. Nguyen, H. H. Lee, and T. W. Chun, "Input Power Factor Compensation Algorithms Using a New Direct-SVM Method for Matrix Converter," *IEEE Trans. Ind. Electron*., Vol. 58, No. 1, pp.232-243, Jan. 2011.

[8] J. D. Zhu, Z. Xu, B. H. Jiang, and C. H. Zhang, "Close-loop control of an AC-DC matrix converter for automotives," *IEEE Electrical Power and Energy Conference (EPEC)*, Vol. 59 , No. 4 , pp. 1939-1949, Oct. 2011.

[9] J. Rodriguez, M. Rivera, J. Kolar, and P. Wheeler, "Areview of control and modulation methods for matrix converters," *IEEE Trans. Ind. Electron*., Vol. 59, No. 1, pp.58-70, Jan. 2012.

[10] K. You, D. Xiao, M. F. Rahman, and M. N. Uddin, "Applying reduced general direct space vector modulation approach of AC/AC matrix converter theory to achieve direct power factor controlled three-phase AC-DC matrix rectifier," *IEEE Trans. Ind. Appl.*, Vol. 50 , No. 3 , pp. 2243-2257, May 2014.

[11] B. Feng, and H. Lin, "Finite control set model predictive control of AC/DC matrix converter for grid-connected battery energy storage application," *Journal of Power Electronics*, Vol. 15, No. 4, pp.1006-1017, Mar. 2015.

[12] X. Liu, Q. F. Zhang and D. L. Hou, "Sliding mode variable structure control of matrix rectifiers," *Trans. of China Electro technical Society*, Vol.28 No.4, pp.149-164, Apr. 2013.

[13] S. Pinto, and J. Silva, "Input filter design for sliding mode controlled matrix converter," *IEEE Power Electronics Specialists Conference*,Vol.2, pp. 648-653, Jun. 2001.

[14] S. Pinto, and J. Silva, "Sliding mode direct control of matrix converters," *IET Electr. Power Appl.*, Vol. 1, No. 2, pp.439-448, Jul. 2007.

[15] Z. P. Wang, Y. S. Mao, Z. H. Hu, and Y. X. Xie, "A sliding mode control design based on the reaching law for matrix rectifiers," *Journal of Power Electronics*, Vol. 16, No. 2, pp. 1122-1130, May 2016.

[16] Z. P. Wang, Y. S. Mao, and Z. H. Hu, "Sliding mode control of uncertain parameter for a matrix rectifier," *IEICE Electronics Express*, Vol. 13, No. 12, pp.20160462, Jun. 2016.

[17] W. B. Gao, Y. F. Wang, and H. Abdollah, "Discrete-time variable structure control systems," *IEEE Trans. Ind. Electron*., Vol. 42, No. 2, pp.117-122, Apl. 1995.

[18] J. J. Kim, J. J. Lee, and K. B. Park, "Design of new time-varying sliding surface for robot manipulator using variable structure controller," *IET Electronics Letters (EL),* Vol. 29, No. 2, pp.195-196, Jan. 1993.

[19] Y. S. Lu, and J. S. Chen, "Design of a global sliding-mode controller for a motor drive with bounded control," *International Journal of Control*, Vol. 62, No. 5, pp.1001-1019, Nov. 1995.

[20] Y. Ni, J. P. Xu, J. P. Wang, and H. K. Yu, "Design of global sliding mode control buck converter with hysteresis modulation," *China Society for electrical engineering*, Vol. 30, No. 21, pp. 1-6, Jul. 2010.

[21] B. Liu, M. Su, X. F. Lin, Y. Sun, and H. Wang, "Reactive power compensation modulation and waveform-improving control strategy for non-isolated H6-type single-phase photovoltaic grid-connected inverter," *China Society for Electrical Engineering*, Vol. 36, No. 4, pp. 1050-1060, Feb. 2016.

[22] IEC 60038:2009, Standard voltages - Part 4: Standard voltages-Highest and lowest voltage values at supply and utilization terminals for a.c. systems having a nominal voltage between 100V and 1000V.

[23] M. M. Polycarpou, and P. A. Ioannou, "A robust adaptive nonlinear control design," *Automatica*, Vol. 32, No. 3, pp. 423-427, Mar. 1996.

[24] H. S. Choi, Y. H. Park, Y. S. Cho, M. H Lee, "Global sliding-mode control. Improved design for a brushless DC motor," *IEEE Contr. Syst. Mag.*, Vol.21, No.3, pp.27-35, Jun. 2001.

Zhanhu Hu was born in Zhanjiang, Guangdong Province, China, in 1965. He received his B.S., M.S., and Ph.D. degrees in Computer Information Systems Engineering and in Computer Application and Aerospace Control Engineering from the Northwestern Polytechnical University, Xi'an, China, in 1988, 1991, and 1999, respectively. From 1999 to 2001, he was a Postdoctoral Researcher in Nanjing. He is presently working as a Professor in the Guangdong Institute of Intelligent Manufacturing, Guangzhou, China. His current research interests include wavelet theory, control engineering and signal processing.

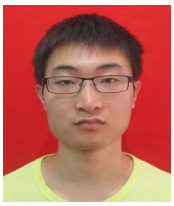

Wang Hu was born in Zhuzhou, Hunan Province, China, in 1992. He received his B.S. degree in Electronics and Engineering from the University of South China, Hengyang, China, in 2015. He is presently working towards his M.S. degree in Electrical Engineering at the Guangdong University of Technology, Guangzhou, China. His current research interests include high-power density rectifiers, multilevel converters, and nonlinear control strategies.

Zhiping Wang was born in Dongguan, Guangdong Province, China, in 1978. He received his B.S., M.S., and Ph.D. degrees in Automation, Software Engineering and Electrical Engineering from the South China University of Technology, Guangzhou, China, in 2001, 2007, and 2016, respectively. He is presently working as a Professor in the Guangdong Institute of Intelligent Manufacturing, Guangzhou, China. His current research interests include high-power density rectifiers and control strategies.

Yunshou Mao was born in Guangzhou, Guangdong Province, China, in 1989. He received his B.S. degree in Electronics and Engineering from the North University of China, Taiyuan, China, in 2013. He is presently working towards his M.S. degree in Electrical Engineering at the Guangdong University of Technology, Guangzhou, China. His current research interests include high-power density rectifiers, multilevel converters and control strategies.

Chenyang Hei was born in Xi'an, Shaanxi Province, China, in 1993. He received his B.S. degree in Electronics and Engineering from the Xi'an University of Technology, Xi'an, China, in 2015. He is presently working towards his M.S. degree in Electrical Engineering at the South China University of Technology, Guangzhou, China. His current research interests include power electronics and control, high-power density rectifiers, active filters, and distributed power quality and control strategies.